LETTERS
PUBLISHED ONLINE: 29 APRIL 2012 | DOI: 10.1038/NGEO1458
nature geoscience

Asymmetric crustal growth on the Moon indicated by primitive farside highland materials

Makiko Ohtake[1]*, Hiroshi Takeda[2], Tsuneo Matsunaga[3], Yasuhiro Yokota[3], Junichi Haruyama[1], Tomokatsu Morota[4], Satoru Yamamoto[3], Yoshiko Ogawa[5], Takahiro Hiroi[6], Yuzuru Karouji[7], Kazuto Saiki[8] and Paul G. Lucey[9]

The Moon's nearside and farside differ in topography[1], crustal thickness[2], mare volcanic activity[3] and elemental concentrations[4]. The origin of this dichotomy is still unclear[5–7]. It is also unknown whether the characteristics of the oldest crust, the anorthositic lunar highlands, reflect a different magmatic evolution of nearside and farside crust. Based on analyses of nearside highland rocks[8,9], it has been suggested that nearside crustal growth occurred from an evolved, iron-rich magma ocean[10], but information from the farside highlands is lacking. Here we apply an empirical algorithm to lunar reflectance spectra[11] from the Kaguya Spectral Profiler and report that magnesium contents relative to iron of primitive crustal highland rocks on the farside are higher than on the nearside. Our findings indicate that the farside crust consists of rocks that crystallized from less-evolved magma than the nearside crust. We conclude that the lunar dichotomy is directly linked to crystallization of the magma ocean and suggest that the composition of the magma ocean was more primitive at the time of crustal growth than previously estimated.

The Moon is globally asymmetric in many properties including topography[1], crustal thickness[2], mare volcanic activity[3] and the concentration of incompatible elements and Fe[4]. Knowing the origin of this lunar dichotomy is important for understanding both the evolution of the Moon and the solidification history of all planetary bodies because its large scale indicates an origin that directly correlates with the early cooling history of a planetary body. However, previous evidence is not able to specify whether the dichotomous features are directly produced by the lunar magma ocean (LMO; refs 6,7,12) or by other secondary processes such as a large impact[13] or mantle overturn[5]. Thus, research has focused on several processes[14] enabling lateral, global transfer of material in an effort to account for the observations, such as heterogeneous accretion of the lunar farside through the very slow impact of a lunar companion[15].

A key geochemical parameter of lunar highland rock for addressing the origin of dichotomy is the Mg# (Mg/(Mg + Fe) in mole per cent) because it provides a degree of differentiation of the magma ocean at the time of its solidification. Here, Mg# is used to discuss the origin of dichotomy and to determine the cooling history of the LMO. In lunar highland rock, Mg#, with the Na content of plagioclase feldspar, separates the anorthosites from more mafic rocks. Most anorthosites exhibit low Mg# relative to other non-mare rocks, with a mean of about 60 and a typical spread of 40–70 (ferroan anorthosite; FAN; ref. 9). The low Mg# imprinted on the few mafic minerals cocrystallizing with the plagioclase is interpreted to be owing to the evolved, Fe-rich nature of the magma ocean at the time of plagioclase crystallization. It provided a melt dense enough for plagioclase flotation[10] (the highland crust is thought to be generated by this mechanism).

However, a few anorthosites[16,17], notably some in meteorites presumably from the lunar farside, exhibit high Mg# (up to 80), which is not consistent with present versions of the magma ocean crystallization model[18] of spatially uniform differentiation processes. Some of the feldspathic meteorites with low abundance in incompatible elements have even higher Mg# (ref. 19), up to 90, though they are thought to be a mixture of FAN and Mg-suite rock (two main rock types of the lunar highland crust) judging from their remelted and metamorphosed texture. The source location and extent of these high-Mg# anorthosites are unknown because of the lack of available data.

Global Mg# can be estimated from Lunar Prospector γ-ray spectrometer data, but those data suffer from a low spatial resolution and a weak Mg signal[20]. Spectral reflectance in near-infrared is also sensitive to the Mg# and it provides an independent measurement of Mg# because of the nonlinear dominance of near-infrared spectra of the Moon by mafic minerals, most notably pyroxene. Here, we present and use an algorithm that derives Mg# from spectral reflectance data to provide a global map of Mg# at high spatial resolution. We focus on FAN because it is believed to be the oldest and most primitive crustal material[9].

We apply this algorithm to the global data set obtained by the Kaguya Spectral Profiler[11], which has spectral coverage from 500 to 2,600 nm in 300 bands and a spatial resolution of 500 × 500 m. We used 26 million spectra after data screening to select data with a high signal-to-noise ratio and low correction errors. We binned these spectra into 1 ° intervals, with 30 km resolution at the equator (Supplementary Fig. S1 and 2). The Mg# algorithm uses spectral absorption angles (Fig. 2b) between 920 and 950 nm that

[1]Institute of Space and Astronautical Science, Japan Aerospace Exploration Agency, 3-1-1 Yoshino-dai, Chuo-ku, Sagamihara, Kanagawa 252-5210, Japan, [2]Department of Earth and Planetary Science, The University of Tokyo, Hongo, Bunkyo-ku, Tokyo 113-0033, Japan, [3]Center for Environmental Measurement and Analysis, National Institute for Environmental Studies, 16-2 Onogawa, Tsukuba, Ibaraki 305-8506, Japan, [4]Graduate School of Environmental Studies, Nagoya University, Furo-cho, Chikusa-ku, Nagoya 464-8601, Japan, [5]The University of Aizu, Ikki-machi, Aizuwakamatsu, Fukushima 965-8580, Japan, [6]Department of Geological Sciences, Brown University, Providence, Rhode Island 02912, USA, [7]Lunar and Planetary Exploration Program Group, Japan Aerospace Exploration Agency, 3-1-1 Yoshino-dai, Chuo-ku, Sagamihara, Kanagawa 252-5210, Japan, [8]Department of Earth and Space Science, Osaka University, 1-1 Machikaneyama, Toyonaka, Osaka 560-0043, Japan, [9]Hawaii Institute of Geophysics and Planetology, University of Hawaii at Manoa, Honolulu, Hawaii 96822, USA. *e-mail: ohtake.makiko@jaxa.jp.

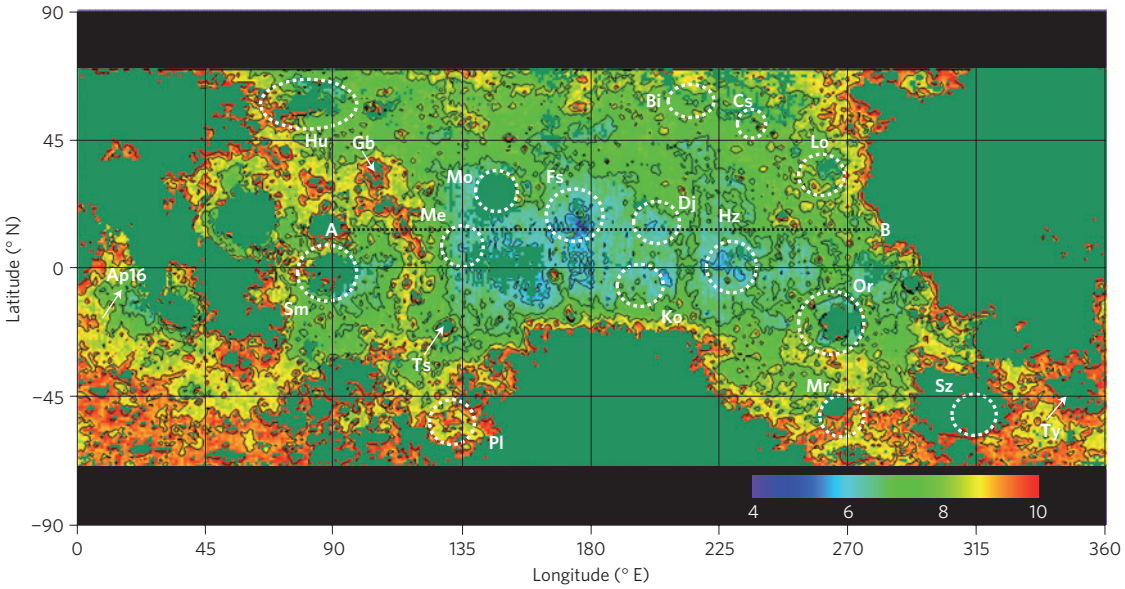

Figure 1 | Mafic mineral abundance (vol.%) of the lunar highlands. Dotted circles denote major basins and arrows denote bright craters in the highland region. Regions with greater than 11 vol.% of mafic mineral abundance and regions with high HCP/LCP ratios (exceeding 0.2) are indicated in sea green. A cross-section (A–B) is presented in Fig. 2c. The contour lines are drawn at intervals of 1 vol.%. The estimated mafic mineral abundance of the Apollo 16 landing site in this study (7.5) matches the average of Apollo 16 FAN measurements (7.0; ref. 9). Ap16, Apollo 16 landing site; Gb, Giordano Bruno; Ts, Tsiolkovskiy; Ty, Tycho; FS, Freundlich–Sharonov; DJ, Dirichlet–Jackson. Other abbreviations for basin names are adopted from ref. 13.

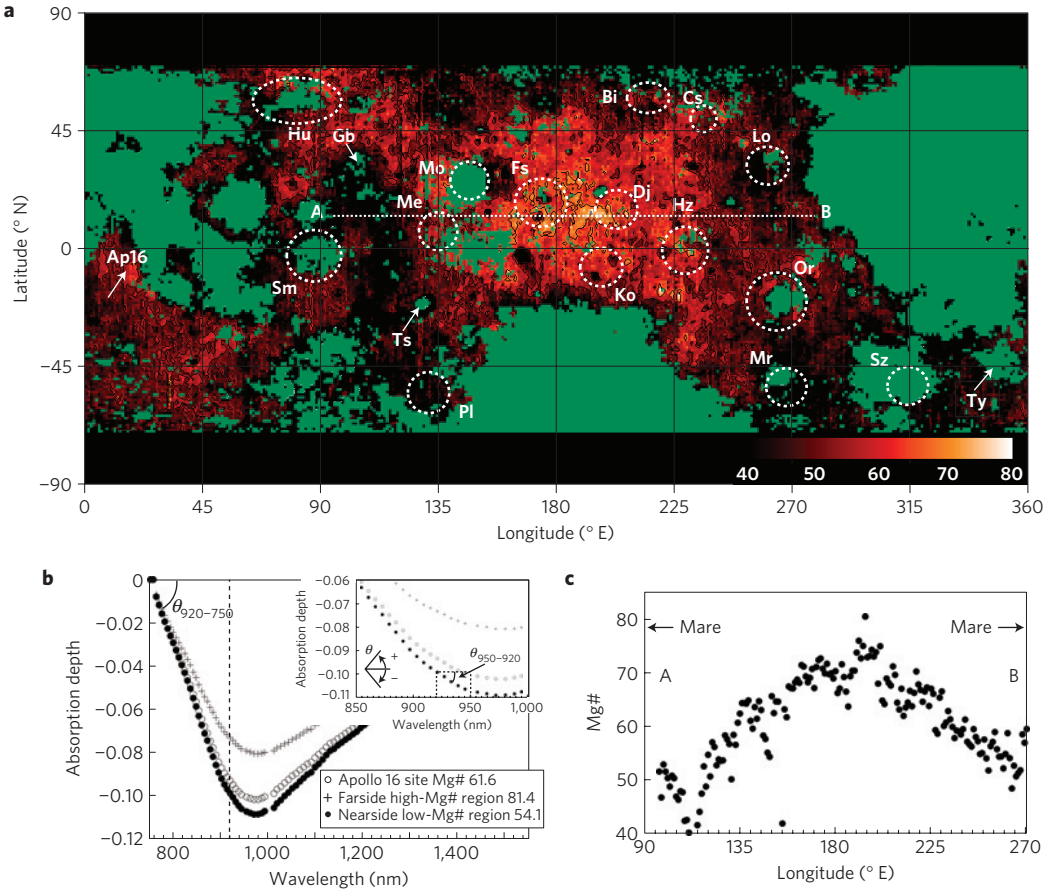

Figure 2 | Mg# of the lunar highlands with representative spectra and example of spatial trend. **a**, The contour lines are drawn at intervals of 10. **b**, Absorption spectra for the Apollo 16 site (−9° N, 16° E), the farside high-Mg# region (13° N, 194° E) and the nearside low-Mg# region (−21° N, 17° E). Schematic images of $\theta_{920-750}$ and $\theta_{950-920}$ (inset) with a definition of $\pm\theta$ are presented. **c**, Mg# trend of cross-section A–B plotted as longitude versus Mg#. Continuous changes of Mg# indicates that a continuous process generated the observed dichotomy of Mg#.

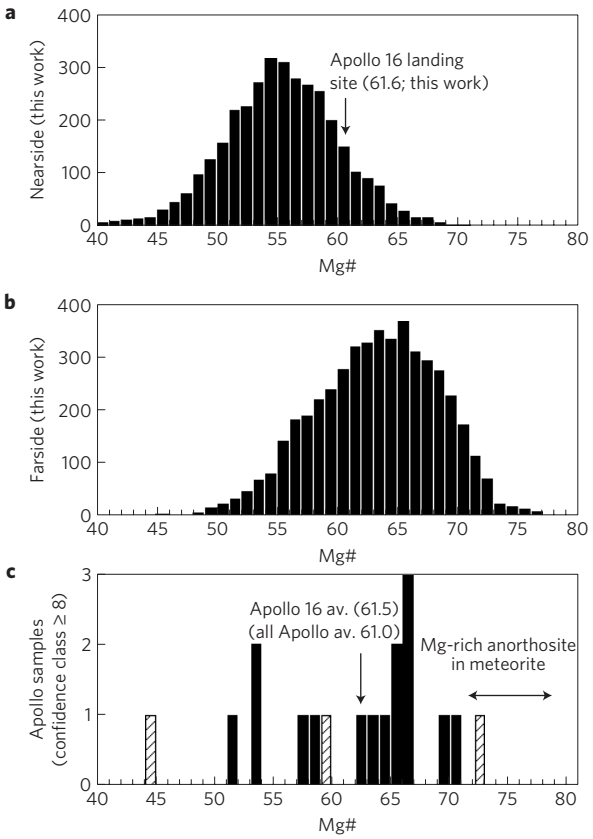

Figure 3 | Mg# histograms of different data sources. **a**, Nearside highlands (including Mg# of the Apollo 16 landing site) and **b**, farside highlands estimated in this study. **c**, Apollo FAN measurements with the Mg# range of rare magnesian anorthosite in lunar meteorites[16,17] indicated. In **c**, the solid columns denote Apollo 16 samples collected in the nearside highlands and the striped columns denote other Apollo samples. The Apollo 16 FAN measurements (average of 61.5) match our estimate (61.6), though FAN measurements are dispersed. The average nearside and farside Mg# differ by 8. Note that the Apollo 16 landing site has higher Mg# than other nearside areas.

are most directly related to the Mg# because the absorption centre wavelength changes with Mg# change in mafic minerals. The angle increases with increasing Mg# in assemblages with low-Ca pyroxene (LCP) as a major mafic mineral component. The Mg# values are derived by applying this algorithm (including mafic mineral abundance correction) to a radiative transfer mixing model[21] of lunar material (Methods section and Supplementary Figs S3–S10). Our algorithm has a ±1 vol.% absolute mafic mineral abundance error, a ±3.5 relative error of Mg# and a −2.0 to +6.0 absolute error of Mg#. The presence of high-Ca pyroxene (HCP) possibly causes large errors in Mg# estimation, but HCP/LCP-uncorrected Mg# is the minimum for each spectra. Therefore, we discuss HCP/LCP-uncorrected Mg# here (Fig. 2a). HCP/LCP-corrected Mg# is presented in Supplementary Fig. S9b.

The derived modal mafic mineralogy of the lunar surface (Fig. 1) indicates that the farside highlands are generally poorer in mafic mineral components (from 5 to 8 vol.%) than the nearside (from 6 to 9 vol.%) in most areas. This dichotomous difference in mafic mineral abundance between the nearside and the farside may have originated from the solidification stage of the crust from the LMO or the mixing of mafic-rich mare material with the highland material on the nearside. We think that the latter case is less likely, as returned highland material from the Apollo 16 landing site, which is quite near the mare region, contained nearly

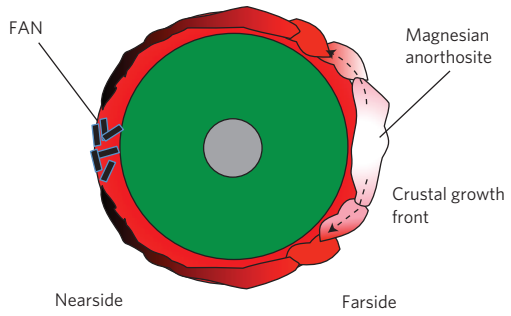

Figure 4 | Plausible dichotomic crustal growth mechanism of the lunar highland crust. A schematic cross-section of a plausible crustal growth mechanism. Colours changing from white to red indicate changes from higher to lower Mg# of crustal material. Grey indicates the core of the Moon; green indicates the mantle. In this model, earlier crystallized, relatively high-Mg# anorthosite rockburgs drift and accumulate in the farside (early stage not shown) and the magnesian anorthosite crust grows towards the nearside (dashed arrows) with Mg# decreasing, and results in FAN crystallizing from the more-evolved LMO in the nearside.

no mare material[22]. Furthermore, there are locations at a similar distance from a mare with considerably different mafic mineral abundance. In addition, we find no increase of the HCP caused by mare contamination in the near-mare locations (Supplementary Figs S9 and S11).

The Mg# distribution (Fig. 2a) of the lunar highlands clearly indicates its dichotomic distribution, with a higher Mg# in the farside highlands (up to 81.4, which indicates relatively primitive material) than in the nearside highlands. Representative spectra presented in Fig. 2b demonstrate that these three spectra have a similar maximum absorption depth of 980 nm with different absorption angles between 920.6 and 944.6 nm (a shallower absorption angle indicates a higher Mg#). The most extensive high-Mg# region is at the centre of the feldspathic highland terrain[4] around the Freundlich–Sharonov and Dirichlet–Jackson basins (F–D region; the brighter area in Fig. 2a), where the lowest abundance of Th (ref. 23) and the maximum crustal thickness[24] were detected by Kaguya γ-ray and gravity observations, though they are not an exact match. This F–D region (from 70 to 81) has higher values than the Mg# range of known Apollo FAN (from 40 to 70) and may have a more primitive composition than FAN. An example of geologic context of one of the highest-Mg# regions has no significant geologic texture, indicating that high Mg# does not originate in a special context but rather is a nature of the regolith of these regions (Supplementary Fig. S12).

Mg# seems to vary continuously from the higher farside to the lower nearside (Fig. 2a and c), indicating a possible continuous Mg–Fe differentiation mechanism rather than a foreign source of the farside highland material[15]. Mare contamination does not account for the dichotomy because the farside Mg# is higher than both FAN and mare basalt. Our nearside estimation is more susceptible to mare contamination, but the Mg# we derived is similar to the Mg# of known FAN without mare contamination. Furthermore, highland material from the Apollo 16 landing site does not indicate sufficient contamination of mare material to explain the observed Mg# (ref. 22). Contamination by high-Mg# (magnesian) basin ejecta from South Pole–Aitken and from other basins is not likely to be the source because the mafic mineral abundance decreases as the Mg# increases toward the highest-Mg# region from the surrounding basin in the farside highlands[25].

As mentioned above, magnesian anorthosites are detected from lunar meteorites[16,17,19]. Magnesian anorthosites as widespread magma ocean flotation cumulates are problematic because of the apparent need for Fe-rich melt to enable plagioclase

flotation[10]. However, the results here indicate that very high plagioclase abundances and high-Mg# mafic minerals occur over vast areas.

We compare our global distributions of Mg# with Apollo sample data (Fig. 3 and Supplementary Fig. S13) including nearside and farside histograms. The average Mg# for the farside highlands in our data is 63.3, which is clearly higher than the nearside average of 55.4; the widths of the distributions are similar. The estimated Mg# of the Apollo 16 landing site in this study (61.6) matches well with the average of Apollo 16 FAN measurements (61.5, Fig. 3c); this result supports the validity of our method. The range of the Mg# histogram for the nearside (42–69; Fig. 3a) matches the previously estimated value based on FAN (ref. 9) and most of the feldspathic lunar meteorite[26] measurements (excluding magnesian anorthosite). The Mg# of the farside ranges from 45 to 81 and its upper limit is comparable to that of the magnesian anorthosite in lunar meteorites (Fig. 3b and c). The average Mg# difference between the nearside and farside (7.9) is comparable to the difference between FAN and magnesian anorthosite in lunar meteorites[17]. The composition inferred from these results is consistent with the suggested farside origin of the magnesian anorthosite[16,17] in meteorites (Fig. 3c) and may explain the relatively magnesian nature of Th-poor feldspathic lunar meteorites[26].

The Mg# of the bulk LMO has not been well constrained[5] because we do not have samples of lunar mantle materials that crystallized during the early cooling stage of the LMO. The higher Mg# in the farside highlands observed in this study indicates higher Mg# of the melt during plagioclase crystallization than previously estimated (23–44) based on FAN compositions[10]. Also, if generation of the highland crust by plagioclase flotation is assumed with no major secondary processes, the higher Mg# of the melt during plagioclase crystallization (which evolved from the bulk LMO) further indicates the possibility of a higher Mg# of the bulk LMO. This possibility is useful for estimating the source material of the Moon relevant to evaluating the suggested impactor origin of the Moon[27] and the giant impact hypothesis[28] as the origin of the Earth–Moon system.

A simple yet plausible model for interpreting our observations is asymmetric crustal growth (Fig. 4). This view is based on a model[6] in which a higher temperature on the nearside caused by thermal shielding by the Earth generates a surface convectional force from the nearside to the farside. During the first stage of crustal formation, plagioclase crystallized and was transported, resulting in relatively high-Mg# anorthosite rockburgs being generated from the less-evolved melt and piled up in the equatorial region on the farside. This was possibly assisted by a surface coriolis force (generated by the Earth's gravity) or other dynamic support and accompanied by efficient segregation of the plagioclase crystal[29]. In the second stage, a FAN crust, which crystallized from the more evolved LMO, forms on the nearside as the crust forms. The relation between anorthosite Mg# and their solidification age must be evaluated in the future[30].

Our identification of the Mg# dichotomy and high-Mg# anorthosite crust in the farside highlands emphasizes the need for study of a new LMO solidification (post-concentric) model.

Methods

Data screening. Data correction and calibration procedures of Spectral Profiler data are described in ref. 11 and in the Supplementary Fig. S1. We used spectra with reflectances exceeding 5% at 752.8 nm at all observed wavelengths to avoid low signal-to-noise ratios and saturated data, phase angles of less than 75° to avoid large errors owing to photometric correction and latitudes below 70° to avoid the effects of shadows for our data analyses.

Averaged 1° × 1° spectra. We binned the screened reflectance spectra into 1 ° intervals, after additional data screening by eliminating irregular reflectances with values exceeding 4 (reflectance at 1,668.3 − average within a bin)/(standard deviation of a bin) to avoid saturated data. The derived spectra correspond to surface regolith spectra. We used 200–900 original spectra to derive the 1 ° binned spectra, enough to consider the averaged reflectances as representative of each location (Supplementary Fig. S1).

Absorption depth for each reflectance spectrum. The continuum is removed from the averaged reflectance (reference for continuum removal is presented in Supplementary Fig. S2) by using 752.8 and 1,547.7 nm as contact points. These wavelengths were selected as an approximation of the contact points for each spectrum. After removing the continuum, we calculated simple moving averages of the absorption to minimize the effect of low noise in the offset mode.

Estimating modal mineralogy and Mg#. The algorithm combines two spectral parameters (the spectral angles of an absorption depth at 752.8 and 920.6 nm ($\theta_{920-750}$), and at 920.6 and 944.6 nm ($\theta_{950-920}$)) that relate to the abundance of mafic minerals and to the Mg# in assemblages with low abundances of HCP. The mafic mineral absorption depth around 1,000 nm increases with the mafic mineral abundance, and the absorption centre wavelength decreases with increasing Mg#. The Mg# values are derived by applying this algorithm to a radiative transfer mixing model that covers the full range of lunar mineralogy and space-weathering effects. The algorithm is not strongly influenced by olivine, which in any case is not abundant at the 30 km scale. First, modelled spectra with different mineralogy parameters were calculated. Calculated parameters are: mafic mineral abundance (2, 4, 6, 8 and 10 vol.%); Mg# (from 50 to 80 in steps of 2); HCP/LCP ratio (0, 0.05, 0.10, 0.15 and 0.20; Mg# in pyroxenes are assumed to be same); and space-weathering degree (metallic Fe content 0.2, 0.4, 0.6, 0.8, 1.0, 1.2, 1.4 and 1.6 vol.%). The modelled grain size of each mineral species was selected as 100 μm both to match the average grain size of lunar regolith and to reproduce the observed spectral parameters of the lunar surface. Second, equations describing the correlation of certain spectral parameters to certain mineralogical parameters were derived (Supplementary Table S1). Third, spectral parameters (OMAT, $\theta_{920-750}$, $\theta_{950-920}$, and HCP/LCP) of the spectra were calculated (OMAT is a parameter to describe the degree of space weathering; reference for OMAT is presented in Supplementary Fig. S3). The observed OMAT values (Supplementary Fig. S7) correspond to a metallic Fe content of 0.9–1.3 vol.%. The HCP/LCP ratio was derived by counting prebinned individual observed spectra having an absorption maximum wavelength longer (HCP) or shorter (LCP) than 980 nm within a 1 ° bin and calculating their ratio. The threshold wavelength of two pyroxenes was selected to derive the upper limit of the HCP content (Supplementary Fig. S8). The presence of HCP in a spectrum results in higher estimated Mg#; therefore, to minimize errors in Mg# estimates caused by the presence of HCP (up to ±5 if HCP/LCP has 0.1 error), we excluded the high-HCP/LCP-ratio region (greater than 0.2) and used HCP/LCP-uncorrected Mg# here (Fig. 2a). Fourth, the observed spectral parameters were applied to the model-derived equations. We estimate that our modal mineralogy has ±1 vol.% absolute error with a ±3.5 relative error of Mg# and a −2.0 to +6.0 absolute error of Mg# (see Supplementary Information for a detailed description of the algorithm errors). Partial melting and crystal growth caused by meteoroid impact after the crust formation may have generated some of the observed LCP. However, our results are still valid because the Mg# values of the newly generated pyroxenes are inherited from their precursors.

Histograms. To generate a histogram of the Spectral Profiler data, we selected a region of mafic abundance less than 8.5 vol.% for the nearside and less than 7 vol.% for the farside. The upper limit of mafic abundance was set 1 vol.% lower than the maximum mafic mineral abundance in the nearside and farside highlands to minimize the effects of mare contamination. We used compiled LCP data from ref. 9 by selecting data on FAN-suite rocks with a higher confidence class (exceeding 8) to generate a FAN sample histogram.

Received 14 October 2011; accepted 2 April 2012; published online 29 April 2012

References

1. Kaula, W. M., Schubert, G., Lingenfelter, E., Sjogren, W. L. & Wollenhaupt, R. Apollo laser altimetry and inferences as to lunar structure. *Proc. Lunar Planet. Sci. Conf.* **V,** 3049–3058 (1974).
2. Zuber, M. T., Smith, D. E., Lemoine, F. G. & Neumann, G. A. The shape and internal structure of the Moon from the Clementine mission. *Science* **266,** 1839–1843 (1994).
3. Head, J. W. & Wilson, L. Lunar mare volcanism: Stratigraphy, eruption, conditions, and the evolution of secondary crusts. *Geochim. Cosmochim. Acta* **56,** 2155–2175 (1992).
4. Jolliff, B. L., Gillis, J. J., Haskin, L. A., Korotev, R. L. & Wieczorek, M. A. Major lunar crustal terranes: Surface expressions and crust-mantle origins. *J. Geophys. Res.* **105,** 4197–4216 (2000).
5. Shearer, C. K. *et al. New Views of the Moon* Vol. 60, Ch. 2, 365–518 (The Mineralogical Society of America, 2006).
6. Loper, D. E. & Werner, C. L. On lunar asymmetries 1. Tilted convection and crustal asymmetry. *J. Geophys. Res.* **107,** 5046 (2002).
7. Wasson, J. T. & Warren, P. H. Contribution of the mantle to the lunar asymmetry. *Icarus* **44,** 752–771 (1980).

8. Wood, J. A., Marvin, U. B., Powell, B. N. & Dickey, J. S. Jr Lunar anorthosites and a geophysical model of the moon. *Proc. Lunar Planet. Sci. Conf.* **1,** 965–988 (1970).
9. Warren, P. H. A concise compilation of petrologic information on possibly pristine nonmare Moon rocks. *Am. Mineral.* **78,** 360–376 (1993).
10. Warren, P. H. Lunar anorthosites and the magma-ocean plagioclase-flotation hypothesis: Importance of FeO enrichment in the parent magma. *Am. Mineral.* **75,** 46–58 (1990).
11. Matsunaga, T. *et al.* Discoveries on the lithology of lunar crater central peaks by SELENE Spectral Profiler. *Geophys. Res. Lett.* **35,** L23201 (2008).
12. Snyder, G. A., Taylor, L. A. & Neal, C. R. A chemical model for generating the sources of mare basalts: Combined equilibrium and fractional crystallization of the lunar magmasphere. *Geochim. Cosmochim. Acta* **56,** 3809–3823 (1992).
13. Wilhelms, D. E. *The Geologic History of the Moon* US Geological Survey Professional Paper 1348 (USGS, 1987).
14. Garrick-Bethell, I., Nimmo, F. & Wieczorek, M. A. Structure and formation of the lunar farside highlands. *Science* **330,** 949–951 (2010).
15. Jutz, M. & Asphaug, E. Forming the lunar farside highlands by accretion of a companion moon. *Nature* **476,** 69–72 (2011).
16. Korotev, L. R., Jolliff, B. L., Zeigler, R. A., Jeffrey, G. J. & Haskin, L. A. Feldspathic lunar meteorites and their implications for compositional remote sensing of the lunar surface and the composition of the lunar crust. *Geochim. Cosmochim. Acta* **67,** 4895–4923 (2003).
17. Takeda, H. *et al.* Magnesian anorthosites and a deep crustal rock from the farside crust of the Moon. *Earth Planet. Sci. Lett.* **247,** 171–184 (2006).
18. McCallum, I. S. A new view of the Moon in light of data from Clementine and Prospector missions. *Earth Moon Planets* **85–86,** 253–269 (2001).
19. Lindstrom, M. M., Knapp, S. A., Shervais, J. W. & Taylor, L. A. Magnesian anorthosites and associated troctolites and Dunitc in Apollo 14 breccias. *Proc. Lunar Planet. Sci. Conf.* **13,** C41–C49.
20. Prettyman, T. H. *et al.* Elemental composition of the lunar surface: Analysis of γ ray spectroscopy data from Lunar Prospector. *J. Geophys. Res.* **111,** E12007 (2006).
21. Denevi, B. W., Lucey, P. G. & Sherman, S. B. Radiative transfer modeling of near-infrared spectra of lunar mare soils: Theory and measurement. *J. Geophys. Res.* **113,** E02003 (2008).
22. McKay, D. S. *et al.* Apollo16 regolith breccias: Characterization and evidence for early formation in the mega-regolith. *Proc. Lunar Planet. Sci. Conf.* **16,** D277–D303 (1970).
23. Kobayashi, S. *et al.* The lowest thorium region on the lunar surface imaged by Kaguya γ-ray spectrometer. *Lunar Planet. Sci.* **41,** abstr. 1975 (2010).
24. Ishihara, Y. *et al.* Crustal thickness of the Moon: Implications for farside basin structures. *Geophys. Res. Lett.* **36,** L19202 (2009).
25. Tompkins, S. & Pieters, C. M. Mineralogy of the lunar crust: Results from Clementine. *Meteorit. Planet. Sci.* **34,** 25–41 (1999).
26. Korotev, R. http://www.meteorites.wustl.edu/lunar/moon_meteorites_list_alumina.htm.
27. Canup, R. M. Simulations of a late lunar-forming impact. *Icarus* **168,** 433–456 (2004).
28. Hartmann, W. K. & Davis, D. R. Satellite-sized planetesimals and lunar origin. *Icarus* **24,** 504–515 (1975).
29. Ohtake, M. *et al.* The global distribution of pure anorthosite on the Moon. *Nature* **461,** 236–240 (2009).
30. Borg, L. E., Connelly, J. N., Boyet, M. & Carlson, R. W. Chronological evidence that the Moon is either young or did not have a global magma ocean. *Nature* **477,** 1–4 (2011).

Acknowledgements

We thank the Kaguya project team and the Lunar Imager/SpectroMeter team members, especially R. Nakamura for useful discussions. Our work was supported by Grants-in-Aid for Scientific Research (KAKENHI; 22540443).

Author contributions

T. Matsunaga, S.Y., Y.O. and Y.Y. calibrated Spectral Profiler data. M.O. conducted data analyses. M.O., H.T., T. Matsunaga, Y.Y., J.H., T. Morota, T.H., R.N., Y.K., K.S. and P.G.L. contributed to writing and improving the paper. All the authors contributed to discussions of the results.

Additional information

The authors declare no competing financial interests. Supplementary information accompanies this paper on www.nature.com/naturegeoscience. Reprints and permissions information is available online at www.nature.com/reprints. Correspondence and requests for materials should be addressed to M.O.